ORIGINAL ARTICLE

Study on dissimilar friction stir butt welding of AA7075-O and AA2024-T4 considering the manufacturing limitation

Pouya Bahemmat · Mohammad Haghpanahi ·
Mohammad Kazem Besharati Givi ·
Kambiz Reshad Seighalani

Abstract In the present article, the effect of friction stir welding (FSW) parameters on the weldability and the characteristics of dissimilar weld of aluminum alloys, called AA2024-T4 and AA7075-O are investigated. A number of FSW experiments are carried out to obtain high-quality welds by adjusting the rotational and welding speeds. The weldability and blending of two materials are evaluated by using the macrostructural analysis to observe whether making a notch in a threaded cylindrical tool will lead to a better blend rather than the threaded taper tool or it will have no effects. The mechanical properties of the welds are studied through microhardness distribution and tensile tests. Furthermore, the microstructure analysis is performed to study the influence of the pin profile and the rotational speed on the grain size. Moreover, in the present study, one of the most major goals is to obtain high-quality welds by spending as little expenditure as possible. Therefore, it prevents using complicated and insupportable high welding speed equipments.

Keywords FSW · Dissimilar joints · Aluminum · Tool geometry · Manufacturing limitation

P. Bahemmat (✉) · M. Haghpanahi
Department of Mechanical Engineering,
Iran University of Science and Technology,
Tehran, Iran
e-mail: bahemmat@iust.ac.ir

M. K. Besharati Givi · K. Reshad Seighalani
Department of Mechanical Engineering, University of Tehran,
Tehran, Iran

K. Reshad Seighalani
Mapna Turbine Blade Engineering and Manufacturing Company
(PARTO),
Tehran, Iran

1 Introduction

Aluminum series 2××× and 7××× are significant classes of alloys widely used in aerospace industry. These classes of aluminum possess high strength and low-weight properties which make them prevailing for industrial applications. AA7000 series alloys are usually chosen for their high strength, while 2000 series alloys are generally designated where fatigue is a challenging problem and for applications where higher service temperatures may be encountered. An important issue that was noticed in the current work is that the forming of AA7075-T6 is more challenging in comparison with the AA7075-O (in the annealed form), and in the manufacture processes and industry, the use of AA7075-O is highly recommended for welding rather than AA7075-T6. It should be noted that the postheat treatment leading to the considered hardness is performed after the welding process.

Generally, the applications of AA7075-O are aircraft fittings, gears and shafts, fuse parts, meter shafts and gears, missile parts, regulating valve parts, worm gears, keys, aircraft, aerospace, and defense applications [1]. Furthermore, the A2024-T4 is mostly used in aircraft fittings, gears and shafts, bolts, clock parts, computer parts, couplings, fuse parts, hydraulic valve bodies, missile parts, munitions, nuts, pistons, rectifier parts, worm gears, fastening devices, veterinary and orthopedic equipment, and structures [2].

In addition to abundant applications of AA7075-O and A2024-T4, the two alloys have a lot of applications in common. As a result, joining these alloys is so much needed in a variety of applications. Therefore, the investigation on welding of AA7075-O and A2024-T4 to obtain high quality joints seems absolutely necessary.

In the current work, regarding the formation limitations of AA7075-T6, AA7075-O has been employed for welding

so that an appropriate heat treatment will be performed after the welding process.

But in these alloys, dendrite structure occurs in the fusion zone due to conventional tungsten inert gas welding and laser welding that leads to a drastic decrease of the mechanical strength [3]. The friction stir welding (FSW) process is a solid-state process. Therefore, the solidification microstructure is absent in the welded metal and the presence of brittle interdendritic and melted phases are restrained [4].

FSW process was first used in 1991 by The Welding Institute (TWI) to join aluminum alloys [5]. FSW is a solid-state welding process in which an inconsumable rotating pin is penetrated into the adjoining edge of the two plates to be welded with a proper tilt angle and then is fed through the joint. The joining of the material is facilitated by severe plastic deformation in the solid state. The generated heat and plastic flow arising from the rotating tool make noteworthy local variations in microstructural mechanical properties [6, 7]. Figure 1 illustrates a schematic diagram of the FSW process. As shown in the figure, during the FSW process performed between two metal plates, one plate is in the advancing side (AS) and the other is located in the retreating side (RS). In the AS, the rotational and welding speeds are in the same direction while at RS, they are in the opposite direction. Bahemmat et al. [8] have studied the dissimilar friction stir welding of AA6061-T6 and AA7075-T6. It was reported that when the weaker alloy is located at the RS, the fabricated weld becomes weaker compared to when the weaker alloy is located at the AS. Therefore, in the present work, AA7075-O is located at the AS and AA2024-T4 at the RS to fabricate welds with more strength.

In FSW, the stir zone (SZ) is placed in the middle and three different regions are detectable on each side. As depicted in Fig. 2, these regions are known as heat-affected zone (HAZ), thermo mechanical affected zone (TMAZ), and base metal (BM).

Several studies have been conducted on friction stir welded butt joints, demonstrating that their strength is very similar to that of the BM and higher than the strength of the joints fabricated by traditional welding techniques [9, 10]. Since base materials do not melt during FSW process, the types of defects which occur in the weld are completely different from those in fusion-based welds. Besides, compared to traditional methods, the FSW retains the capability of providing a weld with lower levels of residual stress and higher strength [11].

In FSW process, parameter selection and tool geometry are key factors which have profound effects on the quality of fabricated welds. Modifying the values of various parameters such as welding speed, rotational speed, attack angle, and pin geometry would lead to an appropriate combination of parameters which could reduce the forces imposed on the tool by the TMAZ segment [12, 13]. Consequently, the quality of the weld is improved when less thermal energy is required to make the material reach the plastic state. Since appropriate plastic flow is responsible for obtaining a weld with high tensile strength and fewer defects, the tool geometry plays a substantial role in achieving a high quality weld.

Geometrical parameters, the height and the shape of the pin, as well as the shoulder surface of the tool affect both the material flow and the frictional heat. Furthermore, the force imposed on the rotating tool during the process has to be chosen properly because the generated pressure on the tool shoulder surface and under the pin lead to the heat generation during the process. Dickerson and Przydatek [14] found that FSW butt joints are generally defect-free if welding process conditions (welding speed and plates thickness) are properly modified within a "tolerance box" for a particular alloy. In spite of this, it is not possible to make the assumption that FSW will be free of flaw due to the fact that manufacturers may want to run FSW outside the tolerance box in order to augment productivity.

Several researches have addressed the relationship between alterable parameters, fatigue characteristics, and mechanical and metallurgic properties of the weld in welding similar aluminum alloys. In 2006, Chen et al. [15] studied the effect of different heat treatments on joining one aluminum series using FSW process. Their research revealed that the base heat treatment of material was clearly related to weld morphologies, weld defects, and tensile attributes of the joints as well as fracture location.

In 2007, Elangovan and Balasubramanian [16] investigated the effect of different tool geometries and rotational speeds on the quality of obtained welds. They employed tensile test and macrostructure analysis to study the relationship between FSW parameters and mechanical properties. It was concluded that the relationship between the static and dynamic volume of pin has an important effect on the quality of the weld.

In 2007, Ren et al. [17] studied the influence of welding speed on microhardness distribution in the cross-section of FSW weld. Moreover, the relationship between the fracture direction during tensile test and hardness distribution was investigated.

In 2008, Gallais et al. [18] focused on developing a coupled model to predict hardness profile during FSW process and evaluated their model for two different heat treatments on base materials by experiment. Their theoretical and experimental results showed that final characteristics of the weld are highly dependent on initial BM characteristics.

In 2009, Reshad Seighalani et al. [19] worked on the effects of the tool material, geometry and tilt angle on FSW of pure titanium. In 2009, Bahemmat et al. [20] investigated
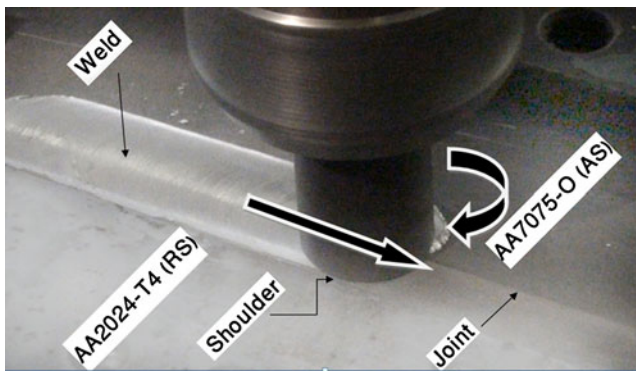
**Fig. 1** Schematic representation of FSW principle

the effect of different rotational speeds and tool pin profiles on mechanical, micro, and macrostructural properties of AA7075-T6 fabricated by FSW. It was recognized that the fracture location is strongly dependent on the hardness distribution. In the present paper, the result is used to justify the fracture location.

Some investigations were also carried out on dissimilar welds. In 2006, Cavalier et al. [21] studied fatigue properties of a dissimilar 2024–7075 joint. They investigated microstructure and precipitate distribution at weld cross-section and fracture surface. Their results showed that FSW decreases fatigue strength but compared to the BM is bearable and presents the FSW as an appropriate joining method for the aluminum alloys.

In 2008, Saad Ahmed Khodir and Toshiya Shibayanagi [22] focused on the microstructure and mechanical characteristics of dissimilar FSW of AA2024-T3 to AA7075-T6. They obtained the maximum tensile strength of 423 MPa at a welding speed of 100 mm/min.

Amancio-Filho et al. [23] used FSW to fabricate the dissimilar aluminum joints of 2024-T351 and 6056-T4 and showed that the weaker component dictated the performance of the joints and fracture occurred in the region of the greatest strength reduction due to annealing phenomena. According to their results, it is predicted that the properties of the weld will be dictated by the AA7075-O in the present work.

In 2009, Priya and et al. [24] investigated the effect of the postheat treatment on the hardness distribution in the weld cross-section. The result was that an appropriate heat treatment can improve the weld characteristics significantly.
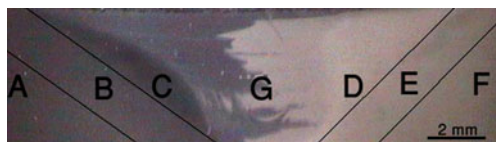
Fig. 2 Different regions of FSW joint *A* BM 7075 at AS, *B* the HAZ at AS, *C* the TMAZ at AS, *D* the TMAZ at RS, *E* the HAZ at RS, *F* BM 2024 at RS, and *G* the SZ

Table 1 Chemical composition (wt.%) of AA2024

Si	0.098
Fe	0.305
Cu[*]	4.490
Mn	0.712
Mg	1.465
Cr	0.016
Ni	0.006
Zn	0.056
Ti	0.112
Pb	0.015
Sb	0.006
Sn	0.013
Zr	0.005
Al	Bal.

Based on this result, the postheat treatment is suggested after the welding process in the present work.

In 2009, Atharifar et al. [25] conducted a remarkable numerical and experimental investigation on the loads carried by the FSW machine during the welding process. They observed that welding speed has a major effect on longitudinal force which is applied to the FSW machine and tool. Their study demonstrated that higher welding speeds cause a higher longitudinal force applied to the FSW machine and tool thus may augment the tool wear and the chance of tool failure. Furthermore, the rotational speed has a major effect on the extent of the lateral and axial force as well as moment applied to the FSW machine. Therefore using higher rotational and welding speed in the FSW process needs more advanced and costly FSW equipments. In spite of the fact that a lot of articles have been published about bimaterials welds, they substantiate dysfunction of using these articles at regular factories as suitable patterns for manufacturing purposes due to usage of high rotational and welding speeds.

Moreover, employing complicated tools and hard materials such as tungsten carbide costs a lot to manufacture the

Table 2 Chemical composition (wt.%) of AA7075

Si	0.331
Fe	0.616
Cu	1.103
Mn	0.014
Mg	2.044
Zn[*]	5.113
Ti	0.027
Cr	0.229
Ni	0.021
Pb	0.011
Sn	0.016
Al	Bal.

Table 3 Mechanical properties of AA2024-T4 and AA7075-O

	Hardness, Vickers	Ultimate tensile strength (MPa)	Tensile yield strength (MPa)	Elongation at break (%)
Mechanical properties of AA2024-T4	137	469	324	19
Mechanical properties of AA7075-O	68	228	103	16

tools stated in those articles. Thus, these complicated patterns are only used at equipped factories.

In the current article, in order to perform FSW process, two different tool geometries called "threaded 4-flute" and "threaded taper" tools are utilized while we take into account the effect of various rotational and welding speeds on the weld characteristics.

The point considered in the design of these tools is that their manufacturing is simple and do not cost much. Thus, they are easily fabricated in all workshops and industrial places. In spite of the fact that tools such as Worl (TM) and MX Triflute (TM) developed by TWI in a wide range of welding speeds produce faultless welds, they are practically very expensive and entail high technologies to be manufactured and are too costly to be regenerated. Thus, if threaded taper and threaded 4-flut tools are able to produce faultless welds, it means that with much lower costs, they have made welds with high mechanical properties. Therefore, one of the aims of this article is considering economical aspects. In addition, in all papers, threaded taper tools have fabricated welds with higher qualities compared to the threaded cylindrical tools. Thus, another aim of this article is to study whether producing a notch in these tools will lead to a better blend of materials in low welding speeds rather than the threaded taper tools.

In the first section, the quality of joints is evaluated by macrostructure analysis and the causes of probable defects are studied. In the next section, the Vickers microhardness distribution by considering diversification in rotational and welding speeds is obtained for each pin profile. Furthermore, peak temperature distribution is measured by utilizing thermocouples installed at a distance of 5 mm from each other on the both sides of the welds. For better comprehension of the temperature and hardness distribution contact, this phase was featured. Then, microstructures and the grain size are analyzed in the welds fabricated by both tools with different rotational speeds and peak temperature is measured at the same rotational and welding speed for two tools in order to compare the heat generation of them. Overall, the results reveals present the impact of FSW tool geometry, as well as rotational and welding speeds on the mechanical and metallurgical properties of the weld. The study of the obtained properties of the fabricated welds shows that the appropriate selection of FSW parameters could lead to an acceptable weld in case of joining dissimilar aluminum alloys.

2 Experimental procedure

AA2024-T4 and AA7075-O aluminum alloys plates with thickness of 5 mm are used in the current study. The plates are located in the butt joint configuration and the welding direction is perpendicular to the rolling direction of both plates. The chemical compositions of AA2024-T4 and AA7075-O are depicted in Tables 1 and 2, respectively. Also, the mechanical properties of AA2024-T4 and AA7075-O are depicted in Table 3. Threaded taper and

Fig. 3 The geometries of tools (**a**) threaded 4-flute tool (**b**) threaded taper tool
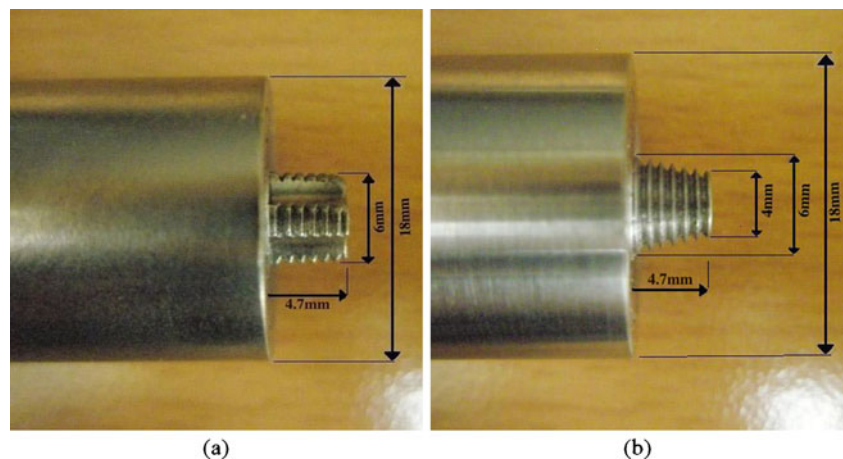
Fig. 4 The apparent defects in the weld: **a** a crack due to low rotational speed, **b** a defect in the hole at the end of the weld due to the high rotational speed

a   b
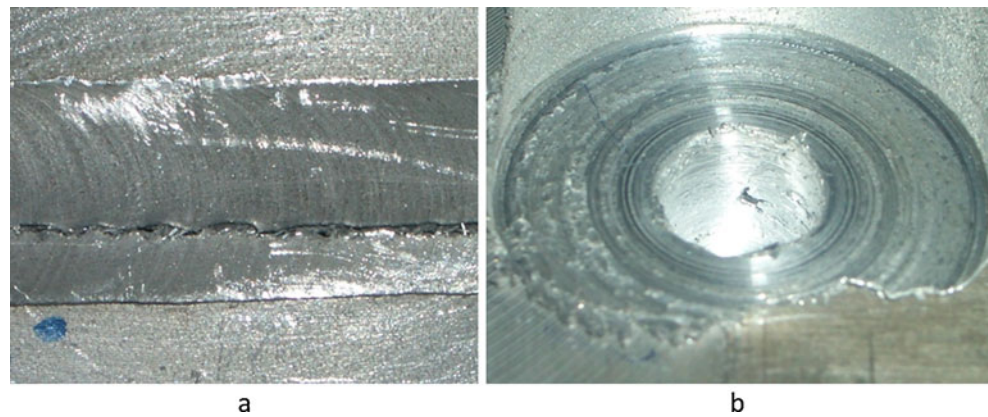
threaded 4-flute tools are utilized to perform the welding process. The dimension of threaded 4-flute and threaded taper tool geometries are demonstrated in Fig. 3.

In 2007, Elangovan and Balasubramanian [26] showed that the ratio of the pin diameter to the shoulder diameter has a profound effect on the quality of welds. It was recognized that the ratio of 3 (shoulder diameter, 18 mm; pin diameter, 6 mm) is the best ratio to produce a high quality weld. As a result, tools with 18 mm shoulder diameter and 6 mm pin diameter are considered at the present study.

As explained before, the current work focuses on employing low-power electromotor and low-welding speeds to fabricate welds in regular factories. To achieve this goal, considering the constant low welding speeds, proper rotational speeds should be selected.

Using a low-power electromotor, an electromotor with the power of 3 kW was selected for the present work. Then, it was seen that as the welding speed increases to more than 100 mm/min, the electromotor starts to tremble. To avoid this problem, the welding speed should be less than 100 mm/min. Therefore, the welding speeds of 50 and 80 mm/min, which are almost reasonable speeds, are selected to fabricate joints by a low-power electromotor.

To choose a range of rotational speeds, it is raised from 200 to 1,800 rpm. It is recognized that as it increases more than 1,100 rpm or decreases to less than 500 rpm, some defects are visible in the appearance of the welds. This is while the welds fabricated with rotational speeds within the range of 500–1,100 rpm are seemed sound apparently and are passed to the next step which is macrostructure analysis. Figure 4 shows two typical apparent defects.

Consequently, two welding speeds of 50 and 80 mm/min are used and for each welding speed, three rotational speeds of 500, 800, and 1,100 rpm are studied. The shoulder penetrates 0.3 mm into the BS and the tilt angle is fixed at 2°. Because installing thermocouples beneath the shoulder

is not practical, during the welding process, infrared camera is used to measure the peak temperature at the SZ and at 800 rpm and 50 mm/min for both tools. Figure 5 illustrates the experimental setup to measure the temperatures. After fabricating joints, the testing specimens are extracted from the welds in the transverse position to the weld line.

In the first step, the specimens are etched in a modified Keller reagent after being polished by a diamond paste. Then, macrostructure photos from the cross-section of welds are taken by optical microscopy. The experiment is followed by Vickers microhardness test under the load of 300 gf for 10 s in 1 mm neighboring distances. For each weld, two specimens are used to determine microhardness profile and the reported results are the average.
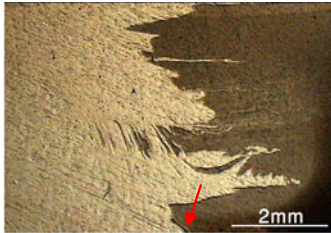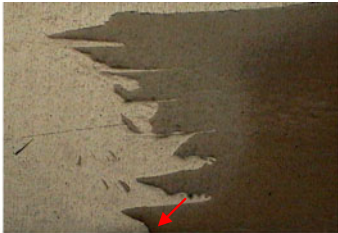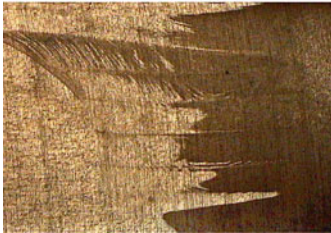
In the next step, the standard of the American Society for Testing and Materials (ASTM) are followed to prepare the specimens for tensile test. These specimens are extracted from the normal direction of the weld line. The specimen is loaded at the rate of 1.5 kN/min as per ASTM specifications.

Finally, microstructure analysis is performed on specimens extracted from a joint for constant welding speed and different rotational speeds. The weld cross-section is etched in the Keller reagent after final polishing for microstructure analysis.
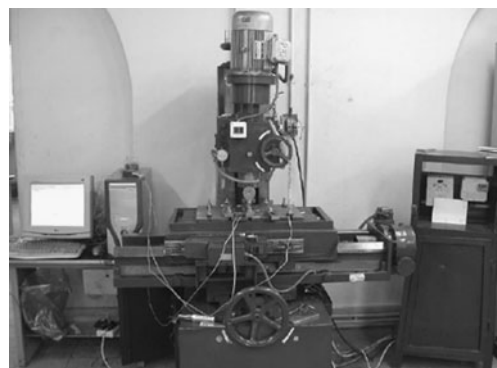
Fig. 5 Setup of the FSW equipment

Fig. 6 Macrostructure figures of weld cross-section for different welding and rotational speeds (threaded taper tool)

Welding speed / Rot. Speed	50 (mm/min)		80 (mm/min)	
	AS AA7075-O	RS AA2024-T4	AS AA7075-O	RS AA2024-T4
500 rpm	a)		d)	
800 rpm	b)		e)	
1100 rpm	c)		f)	

3 Results and discussion

3.1 Macrostructure

Macrostructure observation is the method widely used to detect any major defects which are likely to take place during the FSW process such as crack, pinhole, tunnel defect, and so on. In this section of the study, macrostructures are studied at two magnifications because some defects are not detectable at low magnifications and can be distinguished at higher magnifications. The macrostructures of welds fabricated by threaded taper tools and threaded 4-flute are depicted in Figs. 6 and 7, respectively.
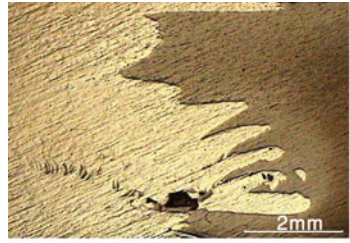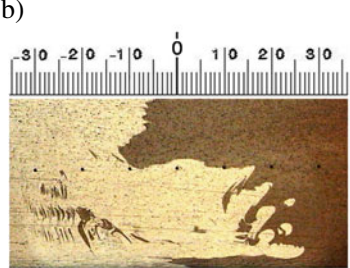
In FSW process, three elements contribute to the formation of the weld. The first one is the temperature in welding region which determines the softening of base metals in the SZ. The second factor is the stirring of plastic materials, the process of amassing multilayer plasticized materials behind the tool, affected by the mutual reaction of rotational and welding speeds and the

pin profile, and the third factor is hot forging of the plastic materials performed by shoulder. If any inappropriate adjustments are set on the aforementioned factors, the fabricated joint will be defective.

In order to control the temperature of welding zone as a crucial factor in weld quality, three various factors could be mentioned. First, the ratio of shoulder diameter to the pin diameter; second, the heat sink occurring due to the forward movement of the tool; and third, the heat generated due to the rotational movement of the tool. In this study, pin to shoulder diameter ratio is equal for both tools and therefore, the determining factors of welding zone temperature are welding and rotational speeds.

According to Fig. 6, in cases a and d, base materials do not adequately plasticized. The reason is the predominance of heat sink over heat generation. Since the weld root has the minimum of stirring, the inadequate softening makes materials not able to be stirred properly. Consequently, some defects will remain in the boundary of two materials around the root. This defect is known as "kissing bond"

Fig. 7 Macrostructure figures of weld cross-section for different welding and rotational speeds (threaded 4-flute tool)

Welding speed / Rot. Speed	50 (mm/min) AS AA7075-O	RS AA2024-T4	80 (mm/min) AS AA7075-O	RS AA2024-T4
500rpm	a)		d)	
800 rpm	b)		e)	
1100 rpm	c)		f)	

defect probably caused by the deepness of inserted pin in the base metals. This defect is characterized by detecting an unwelded portion of butt surface below the SZ [27]. Oosterkamp et al. [28] also have suggested that insufficient break-up of oxide layers in the boundary of two base metals is responsible for formation of kissing bond defect. This
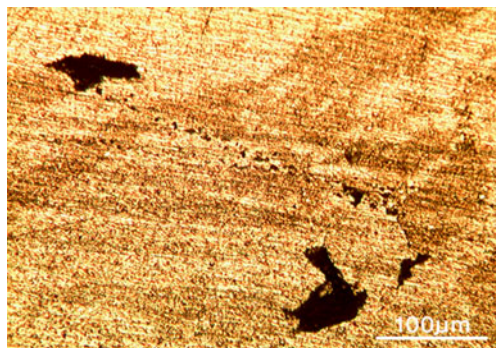
Fig. 8 A defect that observed in higher magnification for specimen 1 (threaded 4-flute tool, 800 rpm, 80 mm/min)

problem can disappear by optimizing the process parameters and specifically by reducing the welding speed and increasing the rotational speed and penetration of the pin in the BM.

In Fig. 7, in case a, d, and e, the low temperature of plasticized material causes higher resistance to the materials against stirring. Moreover, the tool geometry is partially responsible for the observed inappropriate stirring [29]. Since the threaded 4-flute tool cannot produce an effective vertical flow in the plasticized material, in specimen c, the materials are oversoftened due to prevalence of heat generation over heat sink. The high rotational speed of the tool also prompts turbulent flow in the SZ.

Therefore, void defect occurs and this problem is preventable by reducing the rotational speed. Eventually, in specimen f, an undetectable defect at initial magnification is observed in the higher magnification as shown in Fig. 8. Insufficient heat generation is responsible for the formation of this defect since low-plasticized materials resist the forging and stirring.

Table 4 A matrix of defective and sound joints according to the welding and rotational speed for different tools

	Threaded 4-flute tool		Threaded tapered tool	
	50 mm/min	80 mm/min	50 mm/min	80 mm/min
1,100 rpm	Defective	Defective	Sound	Sound
800 rpm	Sound	Defective	Sound	Sound
500 rpm	Defective	Defective	Defective	Defective

In Table 4, sound and defective welds are indicated. According to Figs. 6 and 7, all defects are located at the AS (AA7075-O side) in welds fabricated by threaded 4-flute while in threaded taper case, defects are observed around the joining interval of two metals. All defects of the threaded 4-flute tool case are more crucial compared to those in threaded taper tool case. Thus, it could be inferred from the number of defect free welds and the severity of defects that threaded taper tool is more efficient in fabricating better joints. This section indicated that making notch in the pin of the threaded cylindrical tool does not necessarily affect blending of materials. Therefore, a threaded 4-flute tool will not be a more efficient device compared to threaded taper tool. As a result, to have a

better blending of materials, tapering the pin is more effective than making a notch in it.

3.2 Microhardness and temperature distribution

The microhardness distributions are depicted in Figs. 9 and 10 for threaded 4-flute and threaded taper tools, respectively. Figure 7b shows the path at which hardness test is performed.

In all cases, at the RS, the hardness dwindles by increasing the distance from the weld center until it reaches a minimum value. This point is located at the TMAZ/HAZ interval. After that, the hardness gradually rises by increasing the distance from the weld center and followed by the hardness of AA2024-T4, 130 HV.

Fig. 9 Microhardness distribution in weld cross-section for threaded 4-flute tool (**a**) at welding speed of 50 mm/min and (**b**) at welding speed of 80 mm/min
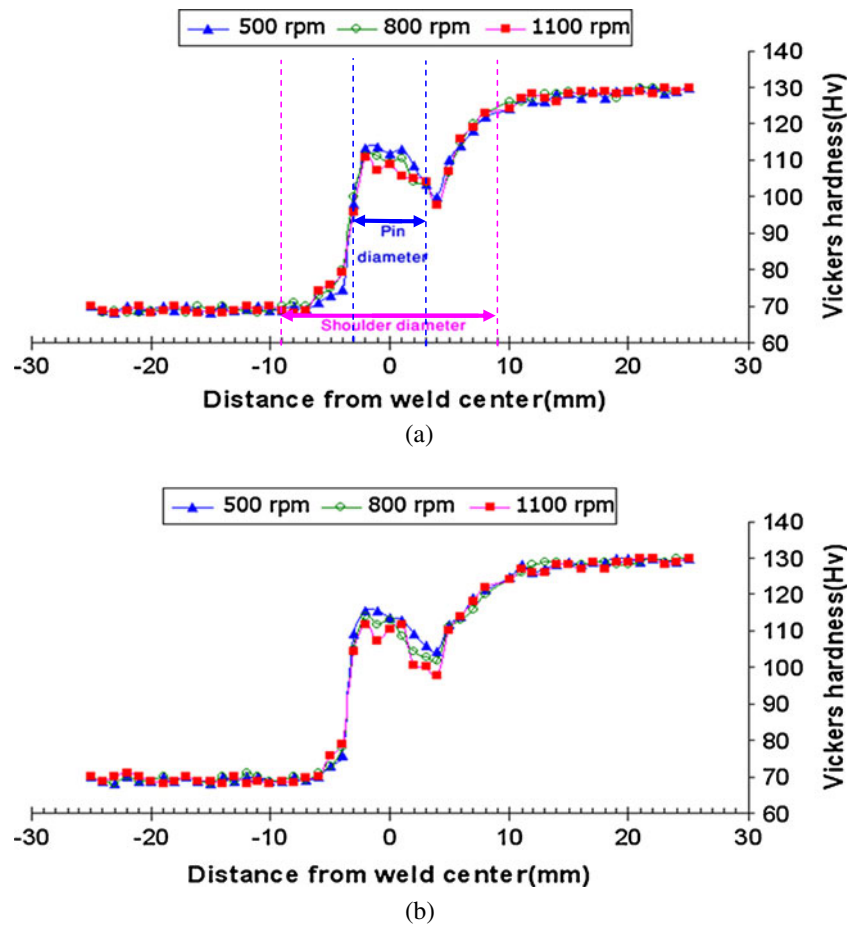
Fig. 10 Microhardness distribution in weld cross-section for threaded taper tool (**a**) at welding speed of 50 mm/min and (**b**) at welding speed of 80 mm/min
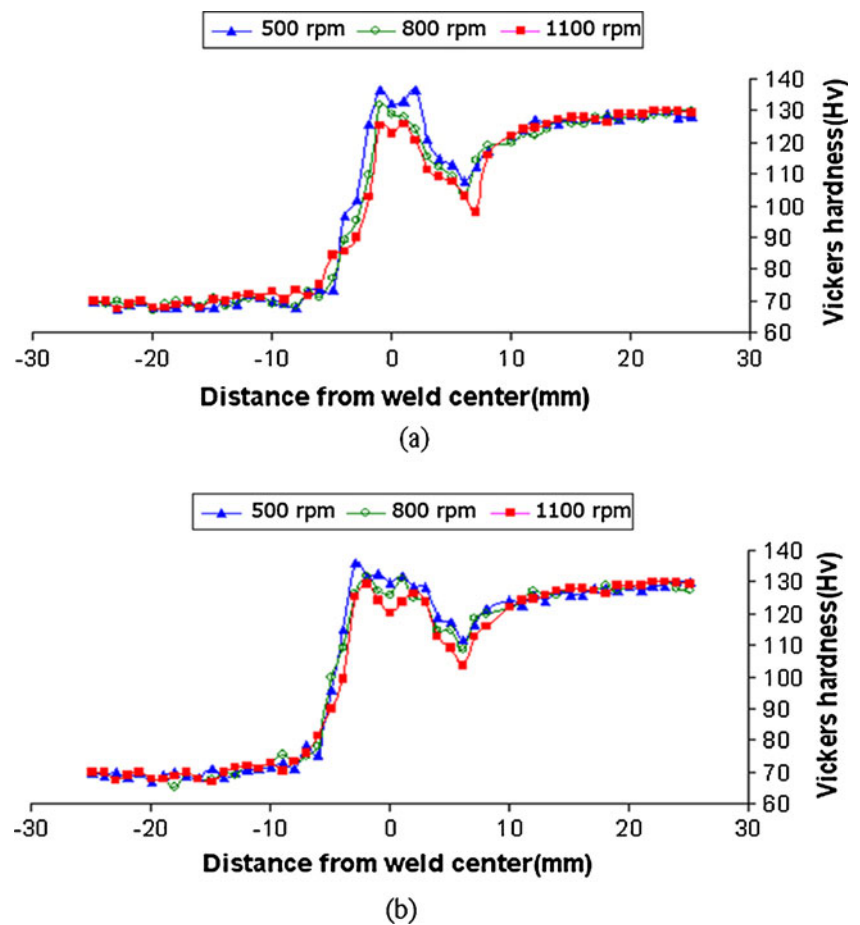
On the contrary, at the AS, where AA7075-O is located in, this minimum point is not observed. In this case, the hardness falls down by increasing the distance from the weld center and reaches a constant hardness of about 70 HV.

To understand the effect of the temperature on the hardness distribution, the peak temperature is measured on both sides of the welds fabricated by the threaded taper tools are acquired. To do this, thermocouples are installed with 5 mm of distance from one another.

Figure 11 shows the temperature distribution for welding speed of 80 mm/min. The peak temperature curve for welding speed of 50 mm/min is illustrated in Fig. 12. According to both diagrams, temperature drops down by increasing the distance from the weld center. Furthermore, the slope of the temperature decrease slows down. At a given transverse speed, the temperature increases by raising the rotational speed and the temperature difference at a given point for different rotational speeds declines by increasing the distance from the weld center. It should also be noticed that, in both figures, at the distance of 10 mm from the weld center, the maximum temperature at the alloy AA2024-T4 is higher than that at the alloy AA7075-O. This can be attributed to the fact that the heat capacity of the alloy 7075-O (cp=0.96 J/gC) is higher than that of the alloy 2024-T4 (cp=0.875 j/gc). Therefore, the amount of the heat required to increase a given degree of temperature of the AA7075-O is higher than the heat required for the AA2024-T4. Furthermore, another parameter which has a major impact on the temperature increase is the plastic work done by the tool. Since Al 7075-O is softer than 2024-T4, the plastic work done on the material by the tool will be less and as a result the provided energy through plastic work per unit volume and the related temperature increase will be less.

The other reason for this is the lower conductivity of 2024-T4 (k=121 w/mk) rather than 7075-O (k=173 w/mk), implying that, heat transfer from a point of 10 mm adjacent to the shoulder falls down with the decrease in conductivity. As a result, the temperature at the point of 10 mm at AA2024-T4 will be more than AA7075-O. In other words, the heat transfer from a point 10 mm adjacent to the shoulder diminishes by decreasing heat conductivity. So, the temperature at 10 mm from the center of the weld at 2024-T4 side becomes higher compared to the other side.

Another essential point is that apart from what was mentioned above is that the temperature almost remains the same at a point of 20 mm in both sides which signifies that

Fig. 11 The peak temperature at welding speed of 80 mm/min for the taper tool
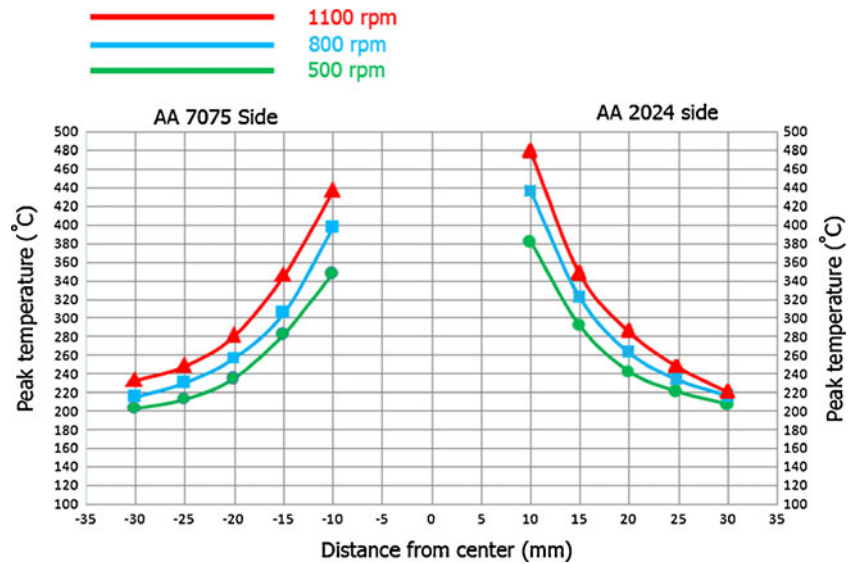

temperature falls much more dramatically in 2024-T4 than 7075-O which can be due to the higher conductivity of 2024-T4 than 7075-O. Generally, when the steady condition is not reached, decrease of the conductivity in two adjacent points leads to the higher temperature difference between them. Therefore, the peak temperature difference at two adjacent points in AA2024-T4 will be more than AA7075-O and as illustrated in Figs. 11 and 12, the temperature falls with a sharper slope at the side of 2024-T4 than 7075-O accordingly.

All in all, alloys AA2024 and AA7075 are both heat treatment-able alloys. Thus, heating or increasing their temperature affects their hardness. The effect of temperature rise on the weld hardness distribution is discussed below.

The normal wrought 2024-T4 product shows rounded as an undissolved excess phase, irregularly shaped particles of unreacted and reaction product along with fine dispersion. The latter causes the grains formed during heat treatment to be moderately elongated or flattened.

In FSW process, the thermo mechanical cycle experienced by the material in the SZ of Al alloys essentially involves hot working. The SZ is subjected to the greatest strain and strain rates as well as the highest temperatures. Combination of these parameters apparently leads to dissolution of the strengthening precipitates as well as continuous dynamic recrystallization. The large grains in the BM are extensively dynamically recrystalized in the SZ due to the great plastic deformation and high temperature

Fig. 12 The peak temperature distribution at welding speed of 50 mm/min for the taper tool
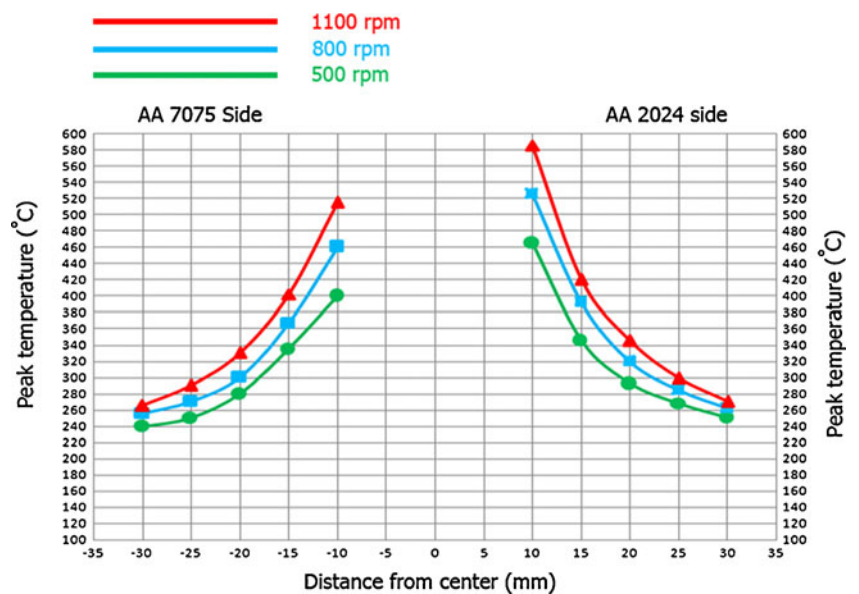
[30] and as formerly mentioned precipitate dissolution and coarsening occurred in the SZ, an important issue which is highly noticeable is that AA2024 and AA7075 are classified into heat-treatable (precipitation–hardenable) alloys and in these alloys the hardness profile is strongly affected by precipitate distribution rather than grain size in the weld. Thus, precipitate dissolution and coarsening make hardness in the SZ less than in the base metals.

In 2024-T4 side, although the TMAZ undergoes plastic deformation, recrystallization does not occur in this zone due to insufficient deformation strain. However, over aging, dissolution and coarsening of some precipitates are obsserved in the TMAZ, due to high-temperature exposure during FSW [31, 32]. The difference between the TMAZ and the SZ is attributable to the grain refinement in the SZ caused by intensive stirring.

Regarding Figs. 11 and 12, at the side of AA2024-T4, the HAZ experiences a peak temperature of about 200–450°C which leads to the over aging and coarsening of the strengthening precipitates in the HAZ and causes the hardness to drop down. But it was reported that the plastic deformation does not usually occur at the point of HAZ [31, 32]. Also the heat exposure decreases and the over aging of strengthening precipitates annihilates gradually by getting further from the welding center and moving toward the BM. As a result, the hardness reaches a constant value.

At the AS, the scattering of strengthening precipitates in the body is akin to that in the HAZ. Therefore, at the AS, a considerable increase in hardness is not expected by getting further from the weld center. The over aging of precipitates, particularly at the HAZ, is directly dependent on the time and temperature of heat exposure in which FSW process is performed. The over aging of precipitates and thereby a decrease in the secondary phases at the SZ substantially reduces the hardness. The hardness profile at the HAZ is correspondent to heat exposure pattern [18]. This heat exposure can be controlled by the adjustment of rotational

and welding speeds. This implies that while the rotational speed increases, the heat exposure increases and when the welding speed increases, the duration of heat exposure shortens followed by observing an increasing pattern in the microhardness profile at the weld region.

As it is clear in Figs. 11 and 12, by increasing the distance from the center of the weld joint, the temperature decreases and due to over aging and coarsening of the precipitates, the hardened particles diminish. According to Figs. 9 and 10, by increasing the distance from the center of the weld, after the point that has the minimum hardness, the hardness increases gradually until it gains a constant value that is the same amount as the hardness of the AA 2024-T4. The trends both of the plots of the peak temperature and the hardness variations are similar and variations occur with the lower slope by increasing the distance.

Comparing Figs. 9 and 10 clarifies that changing the tool geometry from the taper to threaded 4-flute causes the distance of minimum hardness point from weld center to decrease. Thus, it can be inferred that heat exposure of metals in 4-flute tool is less than threaded taper tool because of less friction which will be explained in detail in the microstructure section.

The average of microhardness in the SZ is shown in Fig. 13 for both tools. As perceived, the average in all specimens is greater for threaded taper tool. In addition, an increase in rotational speed or a decrease in welding speed leads to plunging the average of the hardness. The main reason is that in both cases, the temperature and heat exposure duration in the SZ increase. These observations can be directly correlated to the aforementioned elements influential on the hardness in the FSW process.

3.3 Tensile test and fracture locations

In this investigation, the location of fracture is about 18 mm from the weld center in the body of AA7075-O in all defect

Fig. 13 The average of micro-hardness in SZ in weld cross-section for **a** threaded 4-flute tool **b** and threaded taper tool
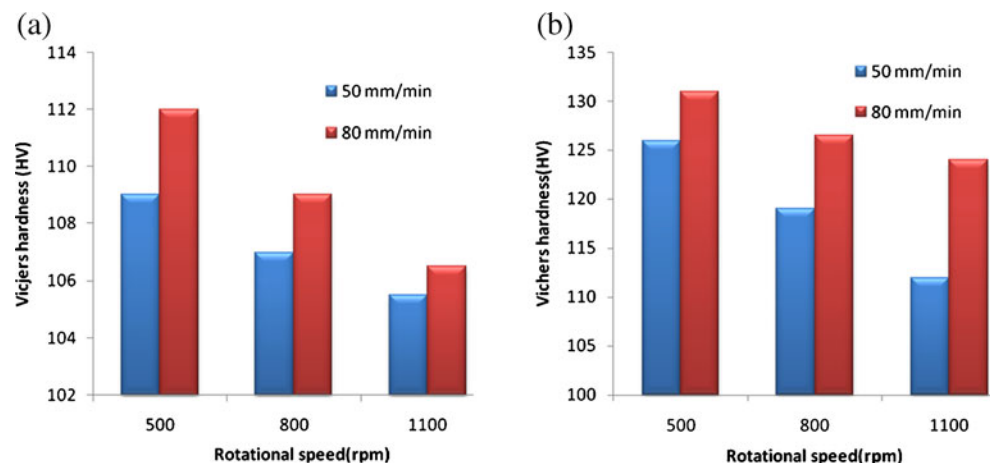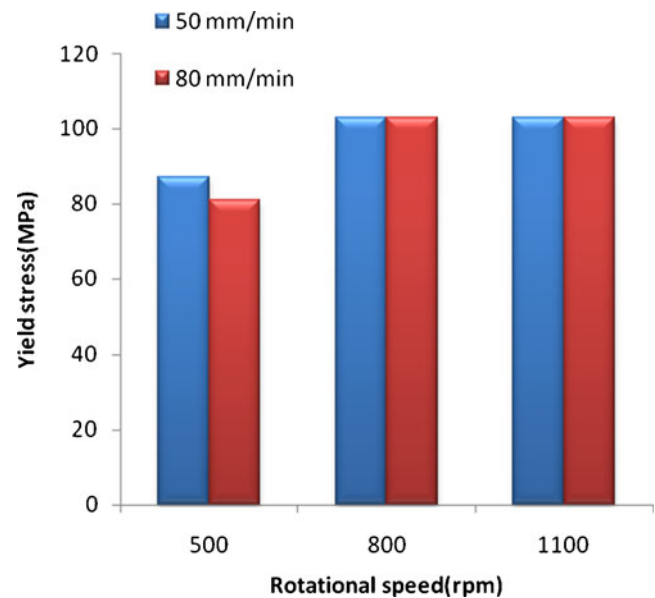
free welds, while in defective welds, except the specimen fabricated by threaded 4-flute tool at the speed of 1,100 rpm and 80 mm/min, fracture occurs at the SZ where the defect exists in. Bahemmat et al. [21] showed that in defect free welds, the determining factor to indicate the fracture location is the microhardness and strength at different regions of the welded plates but in defective welds, the strength or hardness pattern and stress concentration are two essential elements to determine the fracture location. At the SZ, due to the higher hardness in comparison to the body of 7075-O and the HAZ of 2024-T4, in (4-flute tool, the speed of 1,100 rpm, 80 mm/min) specimen, the high strength at the SZ has defeated the small defects in the root of welds and as a result, the fracture occurs in the body of 7075-O which shows the lowest hardness. Still in other defective welds because of size and orientation of defects, stress concentration could defeat the strength at the SZ so the fracture occurred in defects location.

It is likely to observe some small defects at higher magnifications in other specimens categorized as defect free based on initial magnification. It is needed to notice that the fabricated joint has to tolerate enough strength under tensile test and the best strength is observed when the fracture location is either at the BM (in annealed aluminum) or at the HAZ which has low strength in comparison to the SZ. This state is guaranteed when the weld is thoroughly defect free or the influence of stress concentration in defects could not overcome the high strength in the SZ. It should be noted that in all specimens which fractured at the SZ, the fracture cross-section is perpendicular to the tension direction and the welds fractured at BM of 7075-O, have 45° angle at fracture surface. Also, the yield strength (YS) of the welds which fractured at the BM of AA7075-O is about 105 MPa equal to the YS of AA7075-O. Figure 14 illustrates one of the tensile specimens which fractured at the BM.

Figures 15 and 16 show the YS of the welds fabricated by the threaded taper tool and threaded 4-flute tool, respectively. According to the figures, the welds fabricated by the threaded taper tool have larger YS. In addition on average, the specimens fabricated by 4-flute tool and at the speeds of 500 rpm and 80 mm/min illustrated the less resistance under the tensile test. The interesting issue is that the YS of welds fabricated by employing the threaded 4-flute tool are more sensitive to the welding speed in
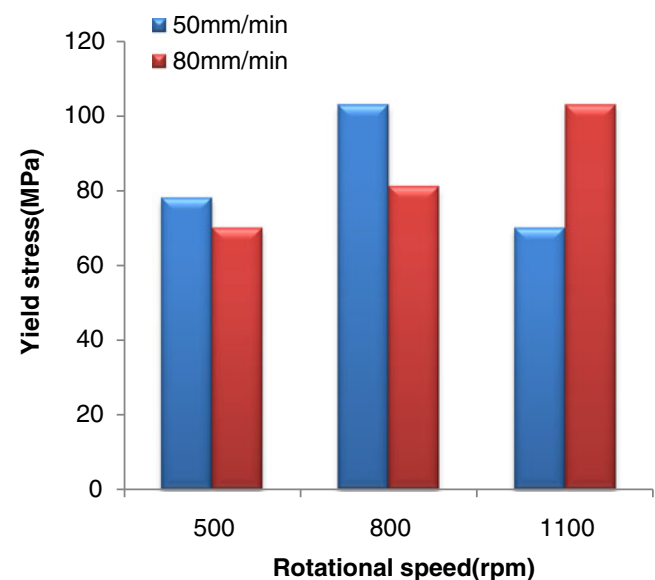
Fig. 15 The tensile test for specimen fabricated by the threaded taper tool

comparison to welds produced by threaded taper tools. In addition, the welds fabricated by the threaded taper tool at rotational speed of 800 and 1100 rpm have more YS.

3.4 Microstructure

Microstructure of the AA2024_T4 and AA7075-O joints are shown in Fig. 17. Figure 17a demonstrates the microstructure of the TMAZ and the HAZ in the AS and Fig. 17b illustrates the microstructure of the HAZ in the

Fig. 16 The tensile test for specimens fabricated by the threaded 4-flute tool

Fig. 14 A specimen which fractured at the BM of AA7075-O

Fig. 17 a The microstructure of
TMAZ and HAZ on AA7075
side and **b** the microstructure of
HAZ on AA2024 side
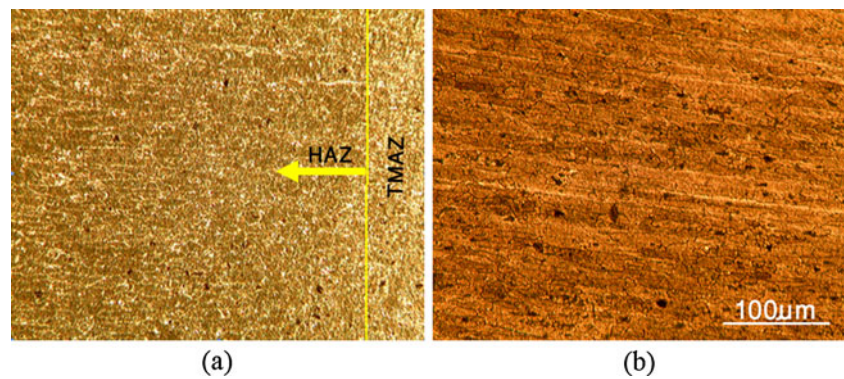
RS. Figure 18 shows the SZ. According to Fig. 18, there are some regions at which the size of the recrystallized grain is smaller compared to other regions at the SZ.

Due to rotational motion of the pin, all the SZ does not deform evenly and at some regions at the SZ, the deformation occurs more than other regions at the SZ. And due to the large deformation, more strain free nucleation sites are created, therefore, the size of the recrystallized grain decreases.

Due to the rotational movement throughout the entire region, the SZ does not experience deformation equally and there are some points that experience more deformation and as a result of a frequent deformation, more strain-free nucleation sites are produced which will cause the size of the recrystallized grain to shrink at these points.

The peak temperature for welding speed of 50 mm/min and rotational speed of 800 rpm is about 470°C and 500°C for taper and 4-flute tools, respectively. This indicates that the taper tool generates more heat compared to the 4-flute tool. The difference in generated heat due to the small difference in peak temperature of both tools is not significant because the main part of heat is produced by shoulder and pin profile does not contribute greatly to the generated heat.

Taper tool case generates higher heat due to the higher contact surface in comparison to the 4-flute tool case, thus the grain size is larger compared to the 4-flute case. Figure 19 depicts the microstructure for welding speed of 50 mm/min and different rotational speeds for both tools. Although the grain size in the SZ in the taper tool case is larger than the 4-flute case, the average hardness in the SZ for the taper tool case is higher than 4-flute tool case as observed in the previous section. The main reason is that the microhardness profile in AA2024-T4 and AA7075-O is more influenced by the size and scattering of precipitating particles rather than the grain size. Elangovan and Balsubramanian [33] showed that the increase in the number of pulses per second leads to a decrease in grain size. The combination of this factor and the temperature increase in the taper tool case causes the grain size to

become bigger. Moreover, according to Fig. 19, the recrystallized grain size can be reduced by decreasing the tool rotation speed at a constant welding speed. The main reason is that higher rotation speed leads to an increase in both degree of deformation and peak temperature of thermal cycle. The increase in the degree of deformation results in a reduction in the recrystallized grain size according to the general principles for recrystallization. On other hand, the increase in peak temperature of FSW thermal cycle leads to generation of coarse recrystallized grains, and also results in remarkable grain growth [34].

4 Conclusions

In this research, the mechanical and microstructural peculiarities of the friction stir-welded dissimilar joints of AA7075-O and AA2024-T4 alloys were investigated.

It is concluded that the heat generation and the heat dissipation patterns which are mainly controllable by adjusting the welding and rotational speeds, were two significant parameters in determining a sound weld. In the research, various combinations of the welding and rotational speeds were used to explore the desired parameters to
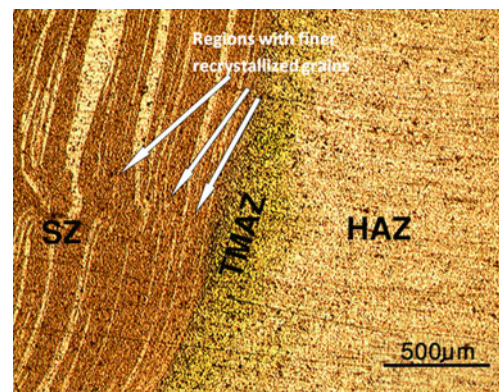
Fig. 18 The microstructure in AA2024 side and indication of regions with finer recrystalized grains
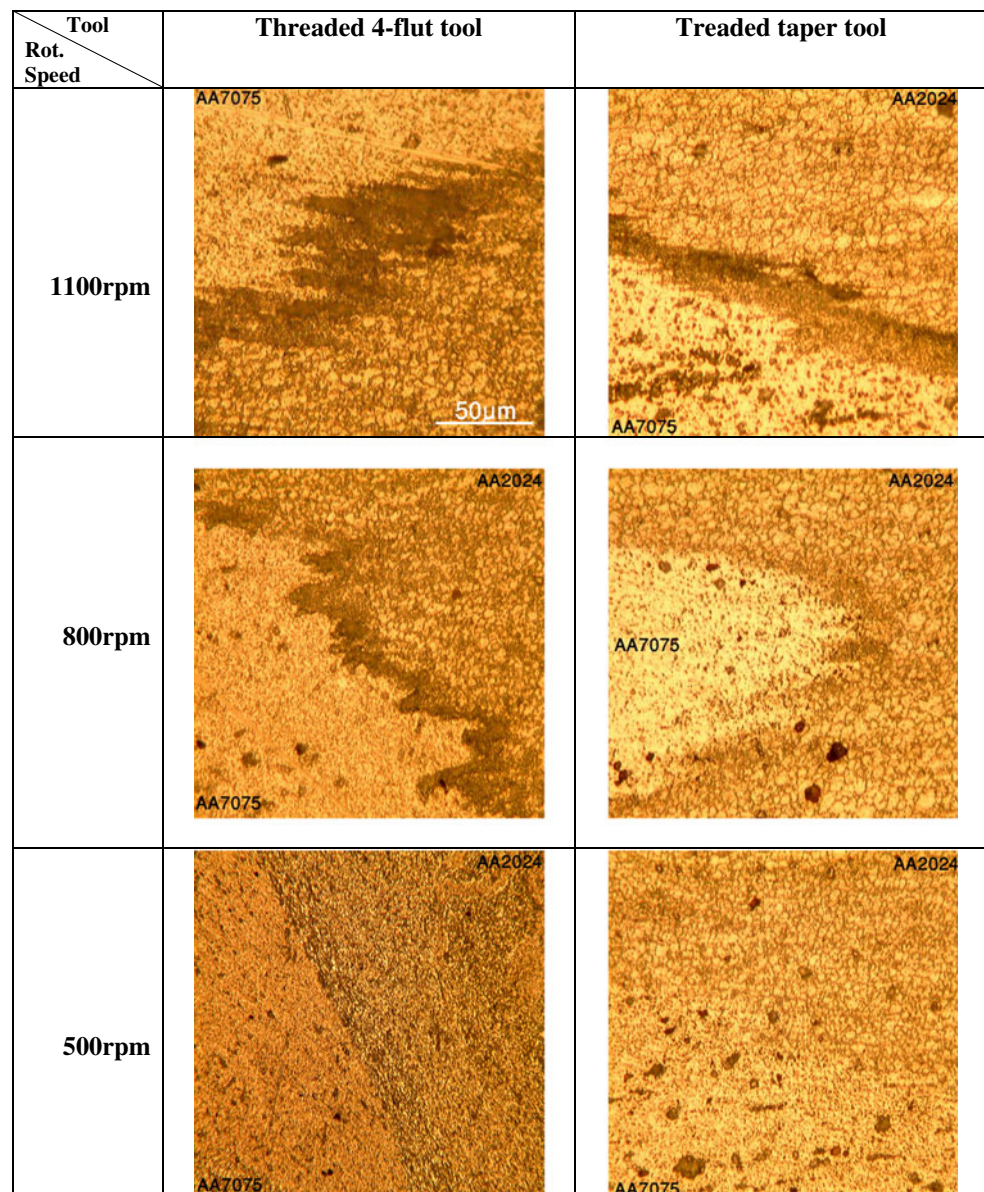
fabricate the joints. In order to identify the weldability, the macrostructural analysis was also performed.

Consequently, it is elucidated that while more defects were noticed in 4-flute tool in AA 7075-O at AS, fewer defects were detected in the root and joint interval fabricated by the taper tool. Then, the hardness distribution for all fabricated welds is obtained and the average hardness was calculated for the SZ. It was clarified that increasing the rotational speed and reducing the welding speed culminated in a decrease in the overall hardness value in the SZ.

Finally, tensile test was conducted on the extracted specimens. In the defective welds, the compromise between stress concentration and strength at the weld zone indicated the fracture location. Thus in the dissimilar FSW joints if any defects are observed at the SZ, there is no evidence to substantiate the fact that it should be crossed out .However, the fracture location in the defect-free welds were at AA7075-O which demonstrates weaker mechanical properties compared to AA2024-T4. So, mechanical varieties of weaker metal are the determining factor of defect-free dissimilar joint properties. Besides, microhardness test reveals that average hardness value in 4-flute tool case was lower and microstructural analysis verified that the grain size in 4-flute tool case was smaller. As a result, the grain size is not the dominating factor of microhardness characteristics in the dissimilar AA7075-O and 2024-T4 joints.

References

1. ASM (1990) Properties and selection: nonferrous alloys and special-purpose materials. ASM, Cleveland, OH
2. Bauccio M (1993) ASM metals reference book. Materials Park, OH, ASM
3. Su JQ, Nelson TW, Mishra R, Mahoney M (2003) Microstructural investigation of friction stir welded 7050-T651 aluminum. Acta Mater 51:713–729
4. Rhodes CG, Mahoney MW, Bingel WH (1997) Effects of friction stir welding on microstructure of 7075 aluminum. Scripta Mater 36:69–75
5. Thomas WM, Nicholas ED, Needham JC, Murch MG, Temple-Smith P, Dawes CJ (1991) friction stir butt welding, GB Patent No. 9125978.8, International patent application No. PCT/GB92/02203
6. Liu HJ, Fujii H, Maeda M, Nogi K (2003) Tensile properties and fracture locations of friction-stir-welded joints of 2017-T351 aluminum alloy. J Mat Proc Tech 142:692–696
7. Rhodes C, Mahoney MW, Bingel WH, Spurling RA, Bampton CC (1987) Effects of friction stir welding on microstructure of 7075 aluminum. Scripta Mater 36:69–75
8. Bahemmat P, Haghpanahi M, Besharati MK, Ahsanizadeh S, Rezaei H (2010) Study on mechanical, micro and macrostructural characteristics of dissimilar friction stir welding of AA6061-T6 and AA7075-T6. P I Mech Eng B-J Eng 224:1854–1864. doi:10.1243/09544054JEM1959
9. Thomas WM, Johnson KI, Wiesner CS (2003) Friction stir welding—recent developments in tool and process technologies. Adv Eng Mater 5:485–490
10. Matrox SJ (2003) Review of fatigue assessment procedures for welded aluminum structures. Int J Fatigue 25:1359–1378
11. Cavaliere P, Panella F (2008) Effect of tool position on the fatigue properties of dissimilar 2024–7075 sheets joined by friction stir welding. J Mater Process Tech 206:249–255
12. Hattingha DJ, Blignault C, Niekerk TI, Jamesa MN (2008) Characterization of the influences of FSW tool geometry on welding forces and weld tensile strength using an instrumented tool. J Mater Process Tech 203:46–57
13. Barcellona A, Buffa G, Fratini L (2004) Process parameters analysis in friction stir welding of AA6082-T6 sheets. Keynote paper of the VII ESAFORM Conference. Trondheim 371–374.
14. Dickerson TL, Przydatek J (2003) Fatigue of friction stir welds in aluminum alloys that contain root flaws. Int J Fatigue 25:1399–1409
15. Chen Y, Liu H, Feng J (2006) Friction stir welding characteristics of different heat-treated-state 2219 aluminum alloy plates. Mater Sc Eng A 420:21–25
16. Elangovan K, Balasubramanian V (2007) Influences of pin profile and rotational speed of the tool on the formation of friction stir processing zone in AA2219 aluminum alloy. Mater Sci Eng A 459:7–18
17. Ren SR, Ma ZY, Chen LQ (2007) Effect of welding parameters on tensile properties and fracture behavior of friction stir welded Al–Mg–Si alloy. Scripta Mater 56:69–72
18. Gallais C, Denquin A, Bréchet Y, Lapasset G (2008) Precipitation microstructures in an AA6056 aluminum alloy after friction stir welding: characterization and modeling. Mater Sci Eng A 496:77–89
19. Reshad Seighalani K, Besharati Givi MK, Nasiri AM, Bahemmat P (2010) Investigation on the effects of the tool material, geometry and title angle on friction stir welding of pure titanium. J Mater Eng Perform 19:955–962. doi:10.1007/s11665-009-9582-8
20. Bahemmat P, Besharati M, Haghpanahi M, Rahbari A, Salekrostam R (2009) Mechanical, micro-, and macrostructural analysis of AA7075-T6 fabricated by friction stir butt welding with different rotational, speeds and tool pin profiles. P I Mech Eng B-J Eng 224:419–433. doi:10.1243/09544054JEM1554
21. Cavaliere P, Nobile R, Panella F (2006) Mechanical and microstructural behaviour of 2024–7075 aluminum alloy sheets joined by friction stir welding. Int J Machine Tools Manu 46:588–594
22. Ahmed Khodir S, Shibayanagi T (2008) Friction stir welding of dissimilar AA2024 and AA7075 aluminum alloys. Mater Sc Eng B 148:82–87
23. Amancio-Filho ST, Sheikhi S, dos Santos JF, Bolfarini C (2008) Preliminary study on the microstructure and mechanical properties of dissimilar friction stir welds in aircraft aluminum alloys 2024-T351 and 6056-T4. J Mater Process Tech 206:132–142
24. Priya R, Subramanya Sarma V, Prasad Rao K (2009) Effect of post weld heat treatment on the microstructure and tensile properties of dissimilar friction stir welded AA 2219 and AA 6061 alloys. Trans Indian Inst Metals 62:11–19
25. Atharifar H, Lin D, Kovacevic R (2009) Numerical and experimental investigations on the loads carried by the tool during friction stir welding. J Mater Eng Performance 18:339–350. doi:10.1007/s11665-008-9298-1
26. Elangovan K, Balasubramanian V (2007) Influences of tool pin profile and tool shoulder diameter on the formation of friction stir processing zone in AA6061 aluminium alloy. Mater Design 29:362–373
27. Sato YS, Takauchi H, Park SH, Kokawa H (2005) Characteristics of the kissing-bond in friction stir welded Al alloy 1050. Mater Sci Eng A 405:333–338
28. Oosterkamp A, Oosterkamp LD, Nordeide A (2004) Kissing bond phenomena in solid state welds of Aluminum alloys. Weld J 205:225–231
29. Zhao Y, Lin SB, Qu FX, Wu L (2006) Influence of pin geometry on material flow in friction stir welding process. Mater Sc Tech 22:45–50
30. Murr LE, Liu G, McClure JC (1997) Dynamic recrystallization in friction-stir welding of aluminum alloy 1100. J Mater Sci Lett 16:1801–1803
31. Mishra RS, Ma ZY (2005) Friction stir welding and processing. Mater Sci Eng R 50:1–78
32. Aydin H, Bayram A, Uguz A, Akay KS (2009) Tensile properties of friction stir welded joints of 2024 aluminum alloys in different heat-treated-state. Mater Design 30:2211–2221
33. Elangovan K, Balasubramanian V (2008) Influences of tool pin profile and welding speed on theformation of friction stir processing zone in AA2219 aluminum alloy. J Mater Process Tech 200:163–175
34. Humphreys FJ, Hotherly M (1995) Recrystallization and related annealing phenomena. Pergamon, New York